River Flow 2010 - Dittrich, Koll, Aberle & Geisenhainer (eds) - © 2010 Bundesanstalt für Wasserbau ISBN 978-3-939230-00-7

The Effect of Coherent Waving Motion on Turbulence Structure in Flexible Vegetated Open Channel Flows

Iehisa Nezu and Taka-aki Okamoto
Department of Civil Engineering, Kyoto University, Kyoto 615-8540, Japan

ABSTRACT: Most aquatic plants are highly flexible and the waving motions of plants are usually observed. The downstream advection of coherent vortices causes the coherent waving of aquatic vegetation, so-called the ‘‘*Monami*’’. The strong oscillations in canopy geometry have the effects of decreasing the amount of vertical turbulent momentum and mass transport into the aquatic canopies. Therefore, hydrodynamic characteristics of vegetated canopy open-channel flows have been investigated intensively, as well as in terrestrial canopy flows. However, the effects of the plant waving motion on turbulence structure have not been revealed as yet. In the present study, the illuminated flow images were taken by CMOS camera (1024×1024pixels) and the simultaneous measurements of water velocity and vegetation motion were successfully conducted by the use of both PIV and PTV techniques. As the results, we revealed the effect of waving motion on turbulence structure in flexible vegetated open-channel flows. The former part of the present study examines the coherent-vortex formulation zones on the basis of the Adrian et al.(2000) ’s detection method. The latter part focused on the relation between coherent structure and the occurrence of Monami phenomena.

Keywords: PIV, Turbulence structure, Monami, Flexible vegetation, Coherent vortex

1 INTRODUCTION

Most aquatic plants are highly flexible and the waving motions of plants are observed usually. The organized vortices are generated by the inflection-point instability and govern the momentum and mass transport. The downstream advection of these coherent vortices causes the coherent waving of aquatic vegetation, referred to as ‘‘*Monami*’’. Therefore, hydrodynamic characteristics of vegetated canopy open-channel flows have been investigated intensively, as well as in terrestrial canopy flows.

Finnigan (1979) has investigated the coherent features of the turbulent velocity fluctuations above and within wheat canopies by hot-wire anemometers and found the resonant waving of wheat stalks referred to as ‘‘*Honami*’’, which corresponds to *Monami* in aquatic waving plants. He revealed then an important role of gusts on mass and momentum transfer toward canopies from the outer boundary layers.

Brunet et al. (1994) have analyzed the distributions of various single-point statistical moments and the velocity spectra in a wind tunnel with waving wheat models by hot-wire anemometers. They showed that the pressure diffusion term in the turbulent kinetic energy (TKE) equation tends to balance with turbulent energy diffusion just above and within the canopies.

Nepf & Vivoni (2000) have conducted turbulence measurements in open-channel flow with flexible vegetation models by using both laser Doppler anemometer (LDA) and acoustic Doppler velocimetry (ADV) and examined the transition between the submerged canopy flow and the emergent canopy flow. They suggested that the flow within a canopy layer could be divided into two zones: the upper layer is called the ‘‘vertical exchange zone’’ and the lower layer is called the ‘‘longitudinal exchange zone’’.

Py et al. (2005) conducted on-site experiments in wheat and alfalfa canopy flows and quantified the motion of a large set of plants by applying a modified PIV technique. They developed a Bi-Orthogonal Decomposition (BOD) analysis of the spatio-temporal velocity fluctuations over the crop canopies and found the large-scale coherent prop

Table 1 Hydraulic condition

Case	Φ	H(cm)	Re	Fr	h(cm)	U_m(cm/s)	Classification of plant motion
F1	0.015	21.0	42000	0.14	7.0	20.0	**Swaying(S)**
F2	0.022						**Swaying(S)**
F3	0.034						**Monami(M)**
F4	0.061						**Monami(M)**
F5	0.137						**Monami(M)**
F6	0.243						**Monami(M)**
R1	0.015	15.0	30000	0.17	5.0	20.0	**Rigid(R)**
R2	0.022						**Rigid(R)**
R3	0.034						**Rigid(R)**
R4	0.061						**Rigid(R)**
R5	0.137						**Rigid(R)**
R6	0.243						**Rigid(R)**

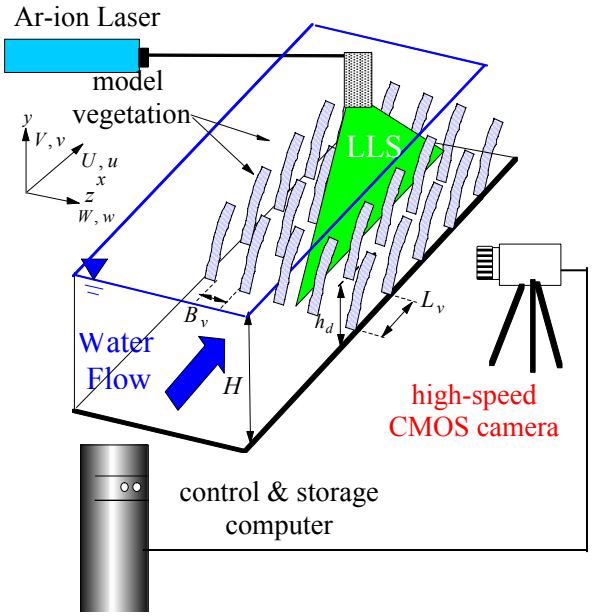

Figure 1 Experimental set-up

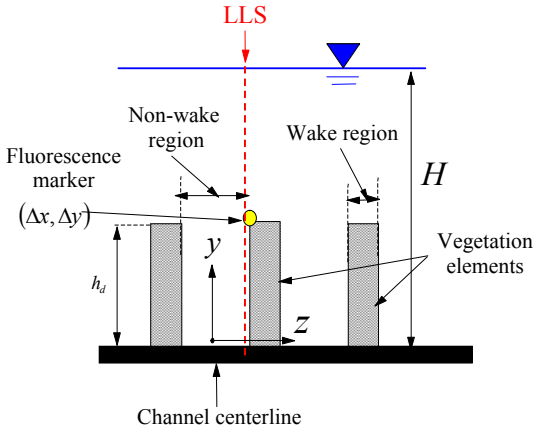

Figure 2 Illuminated PIV plane by LLS

agating structures which scaled with a typical wavelength of wind fluctuations over the canopies.

Ghisalberti & Nepf (2006) conducted flume experiments with rigid and flexible vegetation models and found that the oscillations of the flexible canopies decreased the amount of vertical momentum transfer. They also revealed that the coherent vortex consists of a strong sweep on its front side, followed by a weak ejection on its backside, by using a phase average analysis of the waving motion of vegetation elements.

Zhu et al. (2007) conducted PIV measurements in a wind-tunnel model canopy flow to resolve the flow structure over a wide range of scales. Their quadrant conditional sampling indicated fundamental differences in flow structure, especially between the sweep and ejection events.

Recently, Nezu & Sanjou (2008) observed the large-scale coherent structure near the vegetation edge on the basis of LDA and PIV measurements as well as LES computational simulation. They compared the experimental results with those of terrestrial canopy flows and pointed out the importance of double-averaging method (DAM), i.e., both *time-average* and *space-average*, in the within-canopy layer.

As mentioned above, these vegetated open-channel flows have received much attention for flexible canopies as well as for rigid ones. Flexible canopy flows are more complicated and challenging research topics than rigid canopy flows, because the former should interact with wavings of vegetations in a complicated and organized manner, which are called the Monami phenomena. However, the detailed information on ‘‘Monami’’ phenomena is not yet available, because flow-visualization techniques such as PIV have not sufficiently been applied to these vegetated flows in previous studies. Therefore, the present study examined the interactions between turbulence structure and coherent waving motion in submerged canopy flows with flexible plant models by a combination of PIV and PTV (Particle Tracking Velocimetry). As the results, we revealed the relation between the plant motion and the coherent vortex generated near the vegetation canopies.

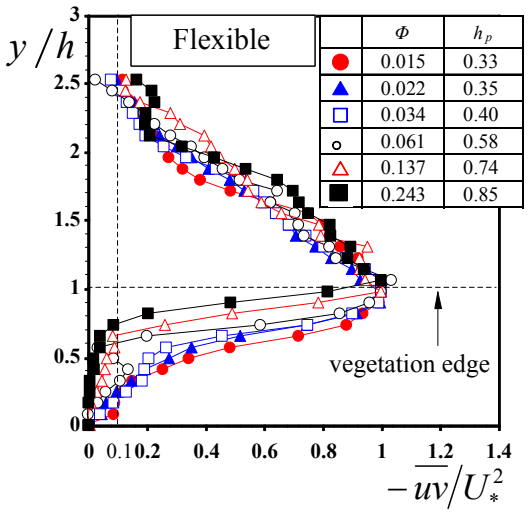

Figure 3 Reynolds stress distribution

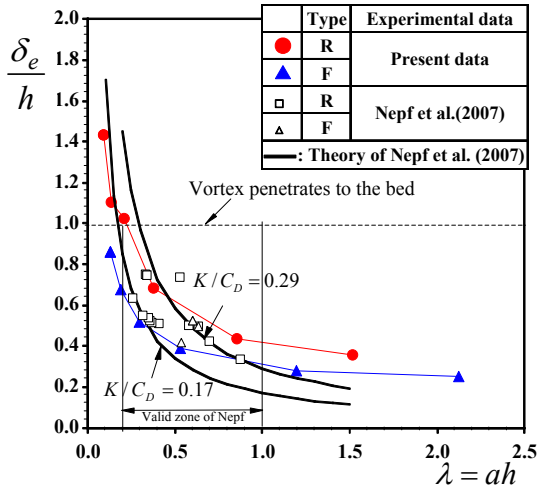

Figure 4 Penetration thickness against the vegetation density

2 EXPERIMENTAL METHOD

Figure 1 shows the experimental setup and the coordinate system. The experiments were carried out in a 10 m long and 40 cm wide tilting flume. The channel slope was changed to create uniform flow conditions. x, y and z are the streamwise, vertical and spanwise coordinates, respectively. The vertical origin, $y = 0$, was chosen on the channel bed. $\tilde{u}(t) \equiv U + u$, $\tilde{v}(t) \equiv V + v$ and $\tilde{w}(t) \equiv W + w$ are the instantaneous velocity components in each coordinate. U, V and W are the time-averaged velocity components and u, v and w are the corresponding turbulent fluctuations.

H is the water depth. The undeflected height h of a flexible vegetation element corresponds to the rigid vegetation height. In contrast, $\bar{h}_d$ is the time-averaged value of the fluctuating deflected height $h_d(t) = \Delta y$ of a typical flexible-vegetation element. The present flexible vegetation was made of h=70mm height, b=8mm width and t=0.1mm thickness OHP film strip sheets. Their flexural rigidity $J \equiv E \times I$ was $J = 7.3 \times 10^{-5}$ [Nm^2], in which E = stiff modulus and I = inertial moment. This value of J was in the same order of magnitude as $J = 1.7 \times 10^{-5}$ [Nm^2] of Velasco et al. (2003) for plastic plant models. The rigid vegetation was modeled as rigid strip plates (h=50mm height, b=8mm width and t=1mm thickness) in the same manner as conducted in laboratory experiments by Nezu & Sanjou (2008).

In the present study, two-components of instantaneous velocity vectors $(\tilde{u}, \tilde{v})$ and the tip positions $(\Delta x, \Delta y)$of flexible vegetations were measured simultaneously by using a combination of PIV and PTV techniques. The illuminated flow pictures were taken by a high-speed CMOS camera (1024×1024 pixels) with 500Hz frame-rate and 60s sampling time. A laser light sheet (LLS) was projected into the water vertically from the free surface. The 2mm thickness LLS was generated by 3W Argon-ion laser using a cylindrical lens. The instantaneous velocity vectors on the x-y plane were calculated by the PIV algorithm for the whole depth region. The instantaneous motion of the flexible vegetation elements was analyzed by PTV technique. The fluorescence marker was attached on the corner edge of the vegetation element, and the LLS was projected on the markers from the free surface (Figure 2).

Table 1 shows the hydraulic condition. Experiments were conducted with both rigid and flexible vegetations on the basis of six flow scenarios, in which the vegetation density $\Phi = ab$ (a is defined as the total frontal area per vegetation volume V, b is the width of the vegetation elements) was changed. The relative submergence depth H/h and the bulk mean velocity U_m were kept constant for all cases. In Table 1, Re $\equiv HU_m/\nu$ is the Reynolds number, and Fr $\equiv U_m/(gH)^{1/2}$ is the Froude number. The classification of plant motions is indicated in Table 1. ‘‘S’’ means *Gently Swaying (non-organized waving)*, and ‘‘M’’ means *Monami (organized waving)*.

3 RESULTS

3.1 *Turbulence* structure

Figure 3 shows the vertical distribution of Reynolds stress $-\overline{uv}$ for flexible vegetation. The friction velocity U_* was evaluated as the peak value of $-\overline{uv}$ (i.e., $U_* = \sqrt{-\overline{uv}_{\max}}$), in the same manner as used by Nezu & Sanjou (2008). The Reynolds stress for flexible vegetation attains maximum near the vegetation edge and the values of $-\overline{uv}$ decrease rapidly in the canopy layer (y/h<1) as the vegetation density becomes larger.

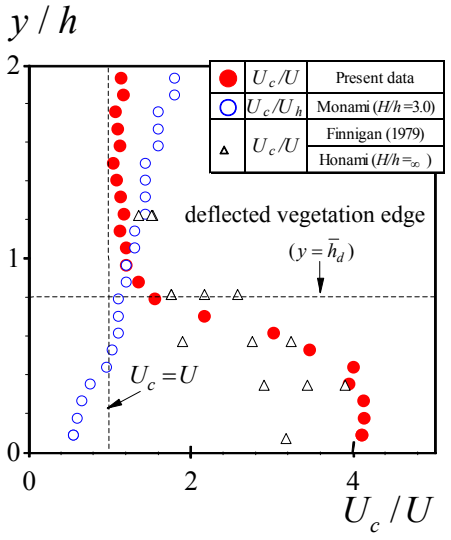

Figure 5 Distribution of convection velocity

These results are consistent with the rigid vegetation data of Nezu & Sanjou (2008)

To evaluate the vertical momentum transfer toward the channel bed quantitatively, Nepf & Vivoni (2000) defined the penetration depth h_p as the elevation of 10% of the maximum Reynolds stress. The values of h_p are indicated in the legend of Figure 3. It is observed that the values of h_p become larger as the vegetation density increases. This implies that the penetration of the Reynolds stress into the canopy becomes smaller for the denser canopies. The momentum transfer from the over-canopy layer toward the bed is obstructed by deflected vegetation elements.

Nepf et al. (2007) also defined the K-H vortex penetration scale δ_e, as follows:

$$\delta_e = \frac{U(h)}{\partial U/\partial y_{y=h}} \tag{1}$$

δ_e implies the mixing-layer thickness, in which the inflection point appears at the vegetation edge. Assuming a turbulence energy balance of large-scale eddies, Nepf et al. (2007) proposed the following relation in a range of $\lambda = ah$=0.2 to 1.0.

$$\frac{\delta_e}{h} = \frac{K}{C_D ah} \tag{2}$$

K is the constant value and C_D is the drag coefficient. Figure 4 compares the penetration thickness δ_e for Rigid and Flexible canopies. The values of δ_e decreases with an increase of the vegetation density $\lambda = ah$ for both Rigid and Flexible canopies, which is consistent with the Reynolds stress properties in Figure 3. It is confirmed that the penetration scale δ_e obeys the theoretical curve of Eq.(2) in a range of λ=0.2 to 1.0. The values of δ_e become larger for Rigid canopy than for Flexible one. Consequently, the penetration of momentum toward the canopy layer is smaller for flexible canopy than rigid one.

3.2 *Detection of coherent eddies*

In the present study, the convection velocity U_c can be evaluated directly from two-point space-time correlation function C_{uu} with no use of Taylor's frozen turbulence hypothesis, as follows:

$$U_c = \frac{\Delta x_{\max}}{\tau} \tag{3}$$

in which, $\Delta x_{\max}$ is the streamwise distance between the reference point and the movable point, at which the correlation becomes maximum when the time lag τ passes.

Figure 5 shows the vertical distribution of the convection velocity $U_c(y)$ for Monami canopy, normalized by the time-averaged mean velocity $U(y)$. For a comparison, Figure 5 also shows the flexible canopy data of Finnigan (1979). The convection velocity U_c of mean eddies is always larger than the local mean velocity U, and the value of U_c/U attains 1.5 at the flexible vegetation edge. The value of U_c/U increases rapidly within the canopy (y/h<1.0), which is in good agreement with terrestrial canopy data by Finnigan (1979). He revealed that when the vortex passes, there is a positive perturbation in the velocity field within the canopy. The positive velocity perturbation may deflect the flexible vegetation elements and, as the results, generates the coherent waving motion of plants (so called "Honami" for terrestrial canopy flows and corresponds to "Monami" for aquatic ones).

Figure 6 shows some examples of instantaneous velocity vectors $(\tilde{u}, \tilde{v})$ at the time t=0.0s, 2.08s and 3.67s for Monami canopy (Φ=0.061). The contours of the streamwise turbulent fluctuations, $u(x,y,t) \equiv \tilde{u} - U$, are shown by color rainbow. High-speed fluid parcel and low-speed fluid parcel are seen clearly, and these large-scale organized parcels are convected downstream. Parcels "A" and "B" in Figure 6 correspond to ejection motions, in which the low-speed fluid is lifted up toward the free surface. On the other hand, parcels "C" and "D" correspond to sweep motions, in which the high-speed fluid is inrushed into the canopy.

On the basis of the Adrian et al.(2000) 's detection method of bursting phenomena in boundary layers, the present study tried to examine coherent eddies. Figure 7 shows the time-series of instantaneous velocity vectors in the PIV plane, which are subtracted by a vortex convection velocity U_c at the vegetation edge. The value of U_c was evaluated from the two-point space-time correla-

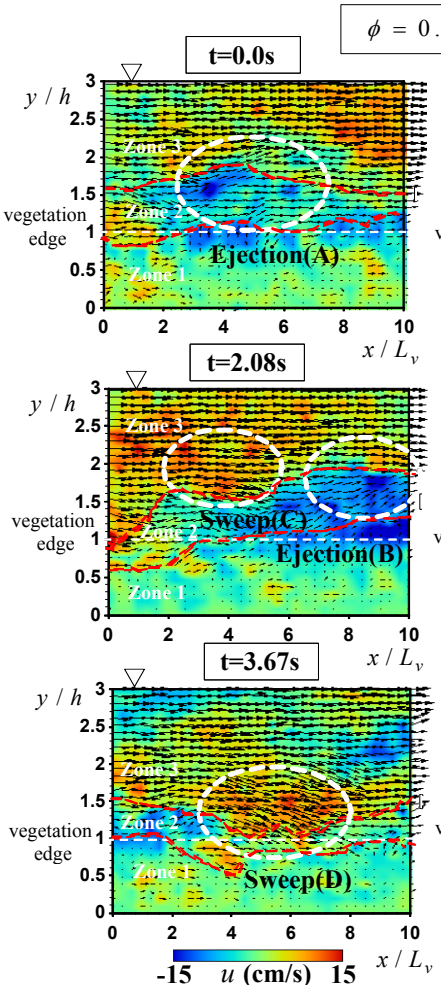

Figure 6 Instantaneous velocity vector

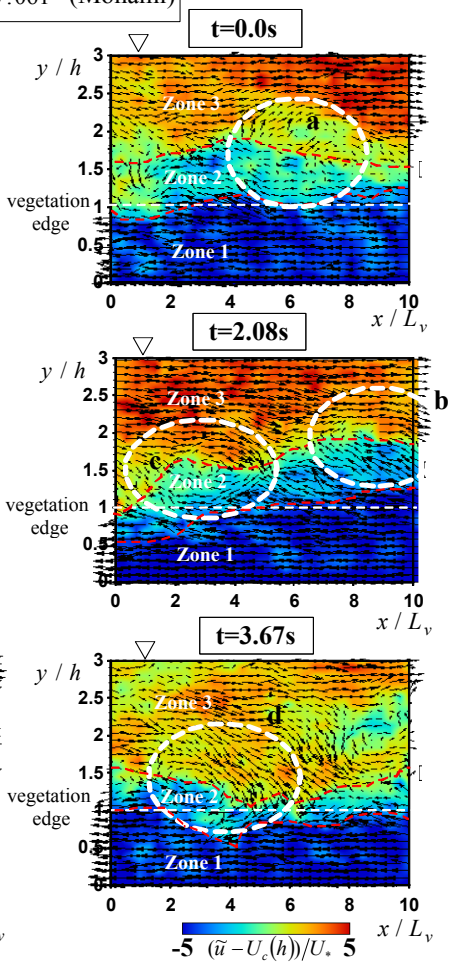

Figure 7 Instantaneous velocity vector subtracted by eddy convection velocity at vegetation edge

tion analysis, as has already been discussed in Figure 5. The $(\tilde{u}-U_c,\tilde{v})$ vectors show vortex-like parcels, which are labeled by 'a', 'b' , 'c' and 'd' in the figure. These parcels are in good agreement with the parcels A, B, C and D, respectively, in Figure 6. This implies that the vortex-like parcels 'a' and 'b' correspond to the ejections, while the vortex-like parcels 'c' and 'd' correspond to the sweeps.

In Figure 6, the uniform momentum zones are separated by hand-drawn lines and labeled Zones 1, 2 and 3(Adrian's method), as follows:

Zone1: $-5<(\tilde{u}-U_c(h))/U_*<-3$
Zone2: $-3<(\tilde{u}-U_c(h))/U_*<1$
Zone3: $1<(\tilde{u}-U_c(h))/U_*<5$

The streamwise velocity component usually changes significantly between zones, but remains roughly constant within a zone. Of particular significance is that the lines pass through the cores of coherent vortices. Such a remarkable coincidence between the vortex core and the boundary between uniform-momentum zones suggests an important association between coherent vortex and uniform-momentum zones. These results are in good agreement with Adrian et al. (2000) in boundary layers.

Figure 8 shows the corresponding instantaneous vorticity Ω, which is defined as

$$\Omega=\frac{\partial\tilde{v}}{\partial x}-\frac{\partial\tilde{u}}{\partial y} \tag{4}$$

Figure 8 contains many regions of concentrated vorticity along the boundaries between the uniform-momentum zones. Some of the weaker fluctuations may be noise in the vorticity measurements, and so we will concentrate on only the strongest regions. The regions labeled a, b, c and d contain the concentrated vorticity. Figure 8 conforms the association between the vortex and uniform-momentum zones, and shows that the coherent vortices produce the regions of large vorticity Ω.

3.3 *Interaction between flow field and vegetation motion*

Importantly, the Monami is visible as the downstream propagation of a localized region of forward plant deflection. Therefore, coherent vortices may induce periodical oscillations in the

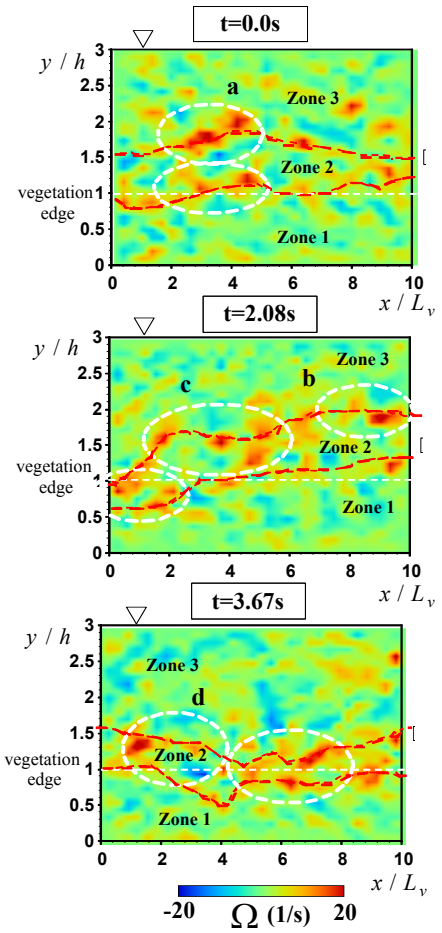

Figure 8 Contour of instantaneous voriticity

streamwise and vertical velocity components near the vegetation edge. Figure 9 (a) shows an example of the power spectrum of the streamwise velocity fluctuations $u(t)$ at y/h=1.3 (above the canopy) for the Swaying and Monami canopies. For the Swaying canopy, no significant spectral peak property is observed. In contrast, for the Monami canopy, a predominant spectral peak f_p occurs near 0.2 Hz. The value of 0.2 Hz for the streamwise velocity spectrum is in good agreement with the value of the theoretical frequency f_{KH} of Kelvin-Helmholtz (K-H) instability proposed by Ho & Huerre (1984) in pure mixing layers, which is given by

$$f_{KH} = \frac{0.032\overline{U}}{\theta} \tag{5}$$

in which, $\overline{U}$ = average velocity of mixing layer and θ = momentum thickness of mixing layer. This good agreement between f_p and f_{KH} was obtained in the other studies for Monami canopies. Ikeda & Kanazawa (1996) and Ghisalberti & Nepf (2002) observed coherent eddies over flexible vegetation canopies and have also obtained the same conclusions.

In contrast, Figure 9 (b) shows the power spectrum of the fluctuations $h_d(t)$ of the flexible vegetation height for Swaying and Monami canopies, which were calculated from the present PTV data. The vibration frequency of flexible vegetation elements is in good agreement with that of the velocity spectral peak f_p and the K-H frequency f_{KH} for Monami canopy. These results imply that the coherent waving motion of vegetation elements is associated with the K-H instability and the large-scale coherent vortices in the mixing-layer zone generate the Monami motion of flexible vegetations. In terrestrial canopy flows, Py et al. (2006) investigated the origin of the instability mechanism by coupling the wind and canopy dynamics. They found that the predominant frequency of wind velocity over the waving canopies matches closely with the free-vibration frequency, i.e. the natural frequency of the wheat plants, and that the flow instability mechanism over plant canopies is driven by a mixing-layer-type instability. The natural frequency f_N of the present flexible vegetation elements was measured using a method proposed by Py et al. (2006), resulting in f_N =0.27 Hz, the value of which is in fairly good agreement with the peak frequency f_p=0.2 Hz of Monami. Figure 9 (b) also confirms that the present classification of

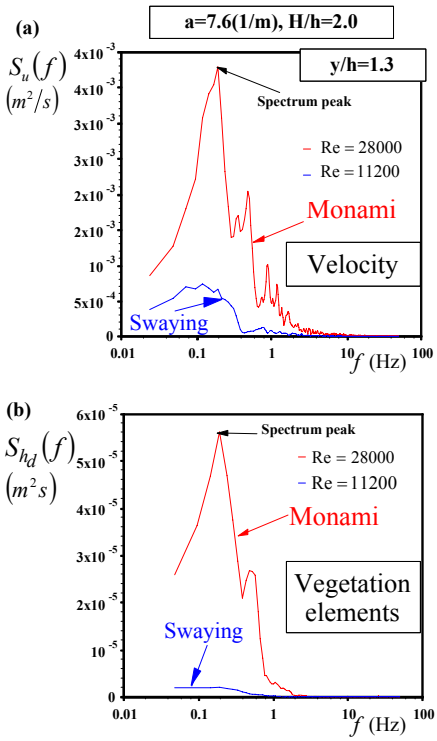

Figure 9 (a) Spectrum of streamwise velocity component u(t) and (b) spectrum of deflected height of vegetation hd(t) for flexible vegetation

the Monami and Swaying by eyes is reasonable in comparison between these two spectra of vegetation fluctuations.

No direct measurements of the Monami phenomena have been conducted quantitatively as yet. To examine the coherent waving motion of flexible vegetation, the space-time correlation $C_{hdhd}(x,\tau)$ between the fluctuations of the deflected vegetation-element heights $h_d(x_0,t)$ and $h_d(x_0+x,t+\tau)$ were analyzed as follows:

$$C_{h_d h_d}(x,\tau)=\frac{\overline{h_d(x_0,t)\times h_d(x_0+x,t+\tau)}}{h'_d(x_0)\times h'_d(x_0+x)} \quad (6)$$

in which, (x_0) = reference point of vegetation and (x_0+x) = movable reference point. h'_d means its r.m.s. value and τ = time lag. $C_{hdhd}(x,\tau)$ for Swaying and Monami canopies are shown in Figure 10. The x-axis plane is normalized by the streamwise spacing of vegetation elements L_v. So, the integer of x/L_v indicates the position of flexible vegetation and thus the distance lag between two vegetation elements. The time lag τ was selected to τ=0.0 s, 1.6 s and 3.2 s. It is evident from Figure 10 that the large values of $C_{hdhd}(x,\tau)$ are observed significantly near the reference point (x/L_v=0.0) for Monami canopy. The correlation peak is convected with an increase of the time lag τ. These results indicate that the waving motions of flexible vegetations are more organized and this coherent waving motion is convected in the downstream direction for Monami canopy than for Swaying one. Py et al. (2005) have conducted similar measurements of flexible canopy motion to detect the local displacements of the crop surface by PIV. They also recognized such a large-scale organized motion of vegetation from space-time decomposition using the BOD analysis.

In contrast, for Swaying canopy (Figure 10 b), the correlation values $C_{hdhd}(x,\tau)$ are much smaller than those for Monami canopy. The convection of the correlation peak is not observed significantly for Swaying canopy, which is coincident with the spectral analysis shown in Figure 9 (b). This

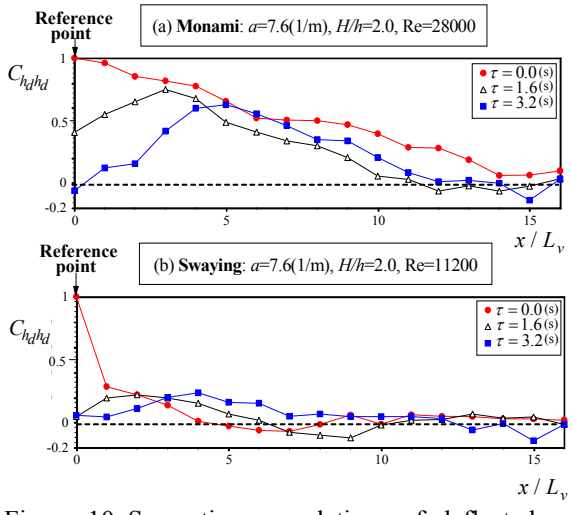

Figure 10 Space-time correlations of deflected vegetation height for (a) Monami and (b) Swaying

suggests that the vegetation elements are independently waving each other, i.e. without organized motions for Swaying canopy.

Table 2 Comparison of flow properties between rigid and flexible vegetation flows

	Rigid	Flexible
Mean velocity U inflection	Yes	Yes
Shear instability	Large	Small
Flow resistance	Large	Small
Mixing-layer velocity profile	Yes	Yes
Reynolds stress	Sharp peak at the vegetation edge	Milder peak
	Larger peak value	Smaller peak value (Monami)
Penetration of momentum	Large	Small
Mean-eddy scale L_x	L_x =1.5h (Large)	L_x =1.0h (Small)
Quadrant Reynolds stress RS	Larger contribution of sweep	Smaller contribution of sweep
Convection velocity U_c	U_c=1.5-2.0U	U_c=2.0U (Monami)
Coherent structure	Large	Small
Mass transport	Large?	Small?

4 DISCUSSION

As mentioned above, the flexibility of the canopy and the presence of Monami affect the mean flow and turbulence structure in the submerged vegetation flow. Table 2 compares several flow properties between Rigid and Flexible vegetation flows. The mean velocity profiles have an inflection point at the vegetation edge (y=h for rigid canopy and y=$\overline{h}_d$ for flexible one), and in the mixing-layer zone, the values of U are approached to the hyperbolic tangent profile both for Rigid and Flexible vegetation flows. In the Rigid vegetation flow, the mean velocity U within the canopy is reduced more significantly and the strong shear layer is produced near the vegetation edge. Consequently, the large-scale coherent vortices at the vegetation edge dominate the vertical momentum transport.

Relative to the Rigid canopy, the values of Reynolds stress $-\overline{uv}$ within the Monami canopy become smaller and the Monami canopy decreases the turbulent momentum transport through the shear layer. The diminished momentum exchange suggests that the coherent vortices become weaker and smaller in the presence of Monami. This suggestion is conformed by the observed mean-eddy length scale L_x. The streamwise and vertical length scales L_x and L_y are larger for the Rigid canopy than for the Flexible canopy. The quadrant analysis implies that the momentum transfer is dominated by sweeps within the canopy and the contributions of sweep events are larger for Rigid vegetation flows. The Monami is observed when the convection velocity U_c of coherent-eddy is significantly greater than the mean velocity U_h at the vegetation edge, as pointed out by Ghisalberti & Nepf (2002). The convection velocity U_c for Monami canopy attains (1.5-2.0)U_h at the flexible vegetation edge and this value is in the same order of magnitude as U_c = 2.0U_h for Rigid canopy. These results suggest that when the canopy is waving, the instantaneous drag distribution may

not be so contributory to the vortex. Consequently, the vortex structure may lose coherence in the presence of Monami.

In particular, effects of flexible canopy on scalar transports, such as various water quality, dissolved gases (O_2 and CO_2) and sediment transport, are not fully investigated as yet. Some researchers suggest that submerged flexible canopies may protect the coastal bed by reducing friction forces near the water-sediment interface, thus, directly protecting the bed from erosive processes. It is further necessary to investigate turbulence and sediment transport within the canopy by simultaneous measurements of velocity and scalar concentration including water temperature.

5 CONCLUSIONS

In the present study, the simultaneous measurements of water velocity and vegetation motion were successfully conducted by the use of a combination of PIV and PTV. As the results, we revealed the relation between turbulence structure and the occurrence of Monami phenomena. Significant results obtained in this study are as follows:

1. We compared the penetration thickness for Rigid and Flexible canopies. The penetration of momentum toward the canopy layer is smaller for flexible than rigid canopies.
2. On the basis of the Adrian et al.(2000) 's detection method, the present study tried to examine coherent-vortex formulation zones. A good coincidence between the center of the coherent vortex cores and the boundary between the uniform-momentum zones clearly demonstrates an association between coherent vortex and uniform-momentum zones.
3. To examine the coherent waving motion of flexible vegetation quantitatively, the space-time correlation between the fluctuations of the deflected vegetation-element heights was analyzed. The large values of space-time correlation were observed significantly near the reference point for Monami canopy. This indicates that the waving motions of flexible vegetations are more organized.

REFERENCES

Adrian, R.J., Meinhart, C.D. and Tomkins, C.D. 2000. Vortex organization in the outer region of the turbulent boundary layer, J. of Fluid Mech, 422, 1-54.

Brunet, Y., Finnigan, J.J. and Raupach, M.R. 1994. A wind tunnel study of air flow in waving wheat: single-point velocity statistics, Boundary-Layer Meteorology, 70, 95-132.

Finnigan, J.J. 1979. Turbulence in waving wheat, Mean statistics and Honami, Boundary Layer Meteorology, 16, 181-211.

Ghisalberti, M. and Nepf, H. 2002. Mixing layers and coherent structures in vegetated aquatic flows, J. of Geophysical Res., 107, 3-1-3-11-

Ghisalberti, M. and Nepf, H. 2006. The structure of the shear layer in flows over rigid and flexible canopies, Environ. Fluid Mech., 6, 277-301.

Ho, C.M. and Huerre, P.1984. Perturbed free shear layers, Ann. Rev. Fluid Mech.,16,365-424.

Ikeda, S. and Kanazawa, M. 1996. Three-dimensional organized vortices above flexible water plants, J. of Hydraulic Eng.,122(11), 634-640.

Nepf, H. M., Ghisalberti, M., White, B. and Murphy, E. 2007. Retention time dispersion associated with submerged aquatic canopies, Water Resource Research, 43, W04422

Nepf, H. M. and Vivoni, E. R. 2000. Flow Structure in Depth-limited, Vegetated Flow, J. of Geophysical Res., 105, 28547-28557.

Nezu, I., and Sanjou. M. 2008. Turbulence structure and coherent motion in vegetated canopy open-channel flows, J. of Hydro-environment Research, 2, 62-90.

Py, C., de Langre, E., Moulia, B. and H'emon, P. 2005. Measurement of wind-induced motion of crop canopies from digital video images, Argic. Forest Met., 130, 223-236.

Py, C., de Langre, E. and Moulia, B. 2006. A frequency lock-in mechanism in the interaction between wind and crop canopies, J. Fluid Mech., 568, 425-449.

Velasco, D., Bateman, A. Redondo, J. and Demedina, V. 2003. An open channel flow experimental and theoretical study of resistance and turbulent characterization over flexible vegetated linings, Flow Turbulence and Combustion, 70, 69-88.

Zhu, W., van. Hout, R. and Katz, J. 2007. On the flow structure and turbulence during sweep and ejection events in a wind-tunnel model canopy, Boundary-Layer Meteorol., 124, 205-233